SUPPLEMENTARY INFORMATION

Permanently polarized hydroxyapatite for selective electroreduction of carbon dioxide towards ethanol

Jordi Sans,[a] Guillem Revilla-López,[a] Vanesa Sanz,[b] Jordi Puiggalí,[a,c] Pau Turon,[*b] and Carlos Alemán[*a,c,d]

[a] Departament d'Enginyeria Química and Barcelona Research Center for Multiscale Science and Engineering, Universitat Politècnica de Catalunya, EEBE, C/Eduard Maristany 10-14, 08019 Barcelona

[b] Research and Development. B. Braun Surgical, S.A.U., Carretera de Terrasa 121, 08191 Rubí (Barcelona), Spain

[c] Institute for Bioengineering of Catalonia (IBEC), The Barcelona Institute of Science and Technology, Baldiri Reixac 10-12, 08028 Barcelona Spain

d Laboratory of the Environmental Center (LCMA), Universitat Politècnica de Catalunya, EEBE, C/Eduard Maristany 10-14, 08019 Barcelona, Spain

E-mail: pau.turon@bbraun.com and carlos.aleman@upc.edu

EXPERIMENTAL METHODS

Materials

Calcium nitrate $Ca(NO_3)_2$, diammomium hydrogen phosphate [$(NH_4)_2HPO_4$; purity > 99.0%] and ammonium hydroxide solution 30% [NH_4OH; purity: 28-30% w/w] were purchased from Sigma Aldrich. Ethanol (purity > 99.5%) was purchased from Scharlab. All experiments were performed with milli–Q water.

Hydrothermal synthesis of hydroxyapatite (HAp)

15 mL of 0.5 M of $(NH_4)_2HPO_4$ in de-ionized water were added at a rate of 2 $mL \cdot min^{-1}$ to 25 mL of 0.5 M of $Ca(NO_3)_2$ in ethanol (with pH previously adjusted to 10.5 using ammonium hydroxide solution) and left aging for 1 h. The whole process was performed under gentle agitation (150 rpm) and at room temperature. Hydrothermal treatment at 150 ºC was applied using an autoclave Digestec DAB – 2 for 24h. The autoclave was allowed to cool down before opening. The precipitates were separated by centrifugation and washed with water and a 60/40 v/v mixture of ethanol – water (twice). After freeze – drying it for 3 days, the white powder obtained was sintered for 2 h at 1000 ºC in air using the Carbolite ELF11/6B/301 furnace.

Thermally stimulated polarization process (TSP)

Mechanical consistent discs of ~1.5 mm of thickness were obtained by pressing 150 mg of previously sintered HAp powder at 620 MPa for 10 min. Thermal polarization was done placing the HAp discs between two stainless steel (AISI 304) and applying 3 kV/cm at 1000 ºC to for 1 h with a GAMMA power supply at 1000 ºC using the same laboratory furnace. The discs were allowed to cool down maintaining the applied

electric potential for 30 minutes, and finally, all the system was powered off and left to cool overnight. Hereafter, the resulting polarized hydroxyapatite is denoted p-HAp.

Characterization

Vibrational spectra for structural fingerprint were obtained by the inVia Qontor confocal Raman microscope (Renishaw), equipped with a Renishaw Centrus 2957T2 detector and a 785 nm laser.

SEM images were obtained using a Zeiss Neon40 microscope equipped with a SEM GEMINI column. All ^{1}H-NMR spectra were acquired with a Bruker Avance III – 400 spectrometer operating at 400.1 MHz and accumulating sixty-four scans. The chemical shift calibration was carried out using tetramethylsilane as internal standard. The samples were dissolved in milli-Q water containing 100 mM of HCl and 50 mM NaCl with the final addition of deuterated water.

Wide angle X-ray diffraction spectroscopy (WAXDS) studies were performed using a Brucker D8 Advance model with Bragg-Brentano 2θ configuration and Cu K_α radiation (λ = 0.1542 nm). A one-dimensional Lynx Eye detector was employed. Measurements were performed in a 2θ range of 25º - 50º in steps of 0.02º, and scan speed of 2 s. The crystallinity (χ_c) was obtained using the following expression:

$$\chi_c = 1 - \frac{V_{112/300}}{I_{300}} \qquad \text{(S1)}$$

where I_{300} is the intensity of the (300) reflection and $V_{112/300}$ is the intensity of the hollow between the (112) and (300) reflections, which disappears in non-crystalline samples.

High-resolution transmission electron microscopy (HRTEM) was performed in a JEOL 2010F microscope equipped with a field emission electron source and operated at

an accelerating voltage of 200 kV. The point-to-point resolution was 0.19 nm, and the resolution between lines was 0.14 nm. Samples were dispersed in an alcohol suspension in an ultrasonic bath, and a drop of the suspension was placed over a grid with holey-carbon film. Images were not filtered or treated by means of digital processing and they correspond to raw data.

p-HAp samples were analyzed using X-ray photoelectron spectroscopy (XPS) XPS on a SPECS system. The spectrometer was equipped with a high-intensity twin-anode X-ray source XR50 of Mg/Al (1253 eV/ 1487 eV) operating with the Al anode at 150 W, placed perpendicular to the analyser axis, and using a Phoibos 150 MCD-9 XP detector. The position of the stage was digitally controlled to ensure that the spot was in the same exact place during the whole treatment. The pass energy of the hemispherical analyzer was set at 25 eV and the energy step of high resolution spectra was set at 0.1 eV. The pressure in the analysis chamber was always below 10^{-7} Pa, and binding energy (BE) values were referred to the C 1s peak at 284.8 eV.

Reactions

A high pressure stainless steel reactor, which was designed *ad hoc*,[S1] was used to perform all the reactions. In brief, the reactor was dotted with a manometer, an electric heater with a thermocouple and an external temperature controller. The reactor was also characterized by an inert reaction chamber coated with a perfluorinated polymer (120 mL) where both the catalyst and water were incorporated. The reactor was equipped with three independent inlet valves for the incorporation of gases and an outlet valve to recover the gaseous reaction products. A UV lamp (GPH265T5L/4, 253.7 nm) was also placed in the middle of the reactor to irradiate the catalyst directly, the lamp being protected by a UV transparent quartz tube. All surfaces were coated with a thin film of a

perfluorinated polymer in order to avoid any contact between the reaction medium and the reactor surfaces, in this way discarding other catalyst effects.

It should be noted that photo/electro/thermal effects on the catalytic behavior were examined using different reaction conditions. More specifically, reactions with and without photocalytic coating as well as with and without UV radiation were conducted to examine the photocatalytic contribution. Besides, reactions using HAp (electrochemically inert) and p-HAp (electroactive), which displays very different electrochemical behavior,[S2] were performed to investigate the electrocatalytic contribution. Finally, reactions at different temperatures allowed to discern the thermocatalytic contribution.

Computational details

The 2 × 1 ×2 HAp supercell was chosen to build the (0001) facet for p-HAp. The latter was built by removing an OH^- orthonormal to the surface from the HAp supercell, which was previously optimized at the chosen DFT level. Consequently, a +1 global charge was applied for all calculations except for those involving formate, unpaired spin being considered when necessary. The initial coordinates of HAp were optimized following the computational details provided below to unwind surface tensions.

The plane waves approach implemented in the Quantum Espresso 4.6 suite of Open-Source computer codes was used.[S3] Calculations were performed at the PBE level of theory[S4] corrected with the Grimme three body dispersion potentials[S5] (PBE-D3), applying the default C_6 software coefficients. A kinetic energy cutoff for the wavefunctions of 40 Ry was employed. A k-point mesh of 3 × 3 × 1 was automatically generated. Instead, a Gamma-centre 1 × 1 × 1 k-mesh was used for calculations of discrete molecules and a 7 × 7 × 7 k-mesh for the bulk HAp calculations. Geometry

optimizations were performed using the conjugated gradient algorithm until both the energy and force variation between consecutive steps was below 10^{-3} a.u and 10^{-4} a.u, respectively. The energy at each step was optimized until the deviation from self-consistency was below 10^{-5} Ry.

Adsorption energies were calculated according to the following process: A + S → AS^*, where A is the adsorbate; S the surface and AS^* the adsorbed state. The adsorption energy (E_{ads}) was be expressed as $E_{ads} = E_{AS*} - (E_A+E_S)$.

S1. M. Rivas, L. J. del Valle, P. Turon, C. Alemán and J. Puiggalí, *Green Chem.*, 2018, **20**, 685–693.

S2. M. Rivas, L. J. del Valle, E. Armelin, O. Betran, P. Turon, J. Puiggalí and C. Alemán, *Chem.Phys.Chem.*, 2018, **19**, 1746–1755.

S3. P. Giannozzi, O. Andreussi, T. Brumme, O. Bunau, M. Buongiorno Nardelli, M. Calandra, R. Car, C. Cavazzoni, D. Ceresoli, M. Cococcioni, N. Colonna, I. Carnimeo, A. Dal Corso, S. de Gironcoli, P. Delugas, R. A. DiStasio Jr, A. Ferretti, A. Floris, G. Fratesi, G. Fugallo, R. Gebauer, U. Gerstmann, F. Giustino, T. Gorni, J. Jia, M. Kawamura, H.-Y. Ko, A. Kokalj, E. Küçükbenli, M. Lazzeri, M. Marsili, N. Marzari, F. Mauri, N. L. Nguyen, H.-V. Nguyen, A. Otero-de-la-Roza, L. Paulatto, S. Poncé, D. Rocca, R. Sabatini, B. Santra, M. Schlipf, A. P. Seitsonen, A. Smogunov, I. Timrov, T. Thonhauser, P. Umari, N. Vast, X. Wu and S. Baroni, *J. Phys.: Condens. Matter*, 2017, **29**, 465901.

S4. J. P. Perdew, K. Burke and M. Ernzerhof, *Phys. Rev. Lett.*, 1996, **77**, 3865–3868.

S5. M. Jonas and S. Grimme, *J. Phys. Chem. C.*, 2014, **118**, 7615–7621.

S6. J. Sans, J. Llorca, V. Sanz, J. Puiggalí, P. Turon and C. Alemán, *Langmuir*, 2019, **35**, 14782–14790.

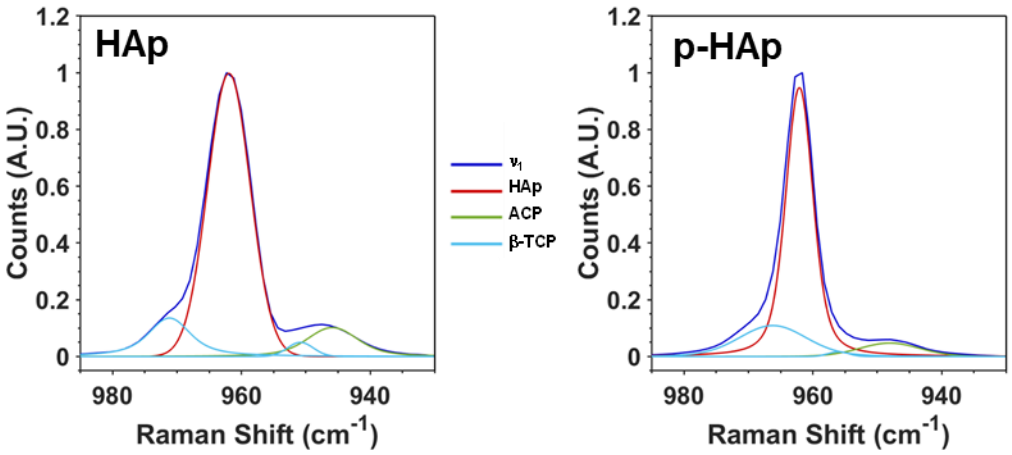

Figure S1. Raman spectra of HAp (left) and p-HAp (right) samples with the deconvolution of the ν_1 peak in the 930–990 cm^{-1} interval. The area of HAp, ACP (amorphous calcium phosphate) and β-TCP (β-tricalcium phosphate) indicates the content of each phase. The content of co-existing phases experiences a reduction in polarized samples (*i.e.* 4.3% and 9.8% for ACP and β-TCP, respectively) that is accompanied by a decrease of the full width at half maximum (FWHM) from 9 cm^{-1} in HAp to 5 cm^{-1} in p-HAp. This result indicates an increase of the HAp phase by means of a reduction of crystal imperfections, such as PO_4^{3-} tetrahedrons distortions.

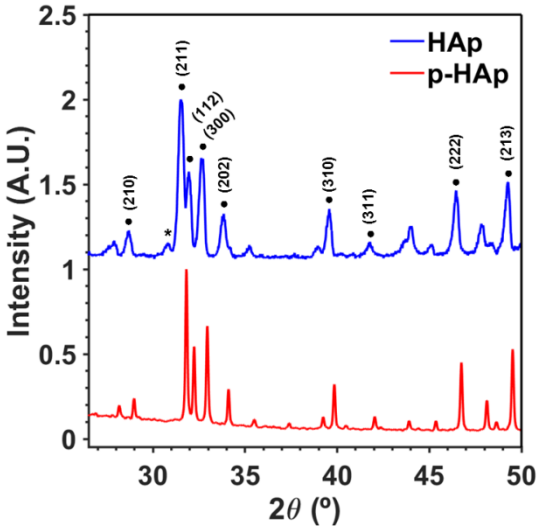

Figure S2. WAXDS spectra of HAp and p-HAp samples. The main reflections of HAp are depicted (JCPDS card number 9-0077). Accordingly to the Raman studies, the polarization treatment results in a significant enhance of crystallinity (χ_c) and reduction of β-TCP (the main peak located at 2θ= 31.5 º, JCPDS card number 9-0432, has been marked with a *) can be observed. Indeed, χ_c= 0.83±0.03 and 0.94±0.02, for HAp and p-HAp, respectively.

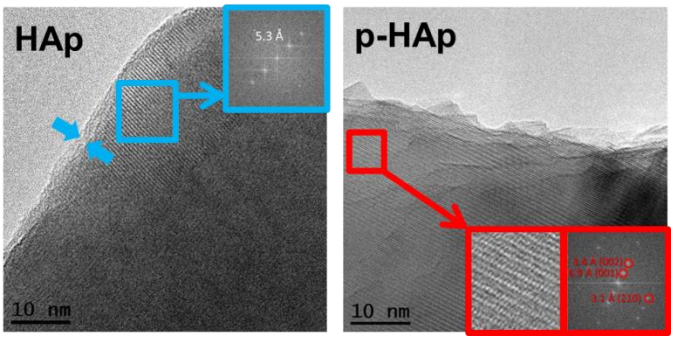

Figure S3. HRTEM studies comparing HAp and p-HAp samples confirm the conclusions derived from WAXDS and Raman spectra. A reduction of crystal imperfections (i.,e amorphous layer highlight with blue arrows and β-TCP phase) at the surface can be observed for p-HAp sample. Accordingly, well defined fringes can be observed for p-HAp, which have been associated to the (001), (002) and (210) crystallographic planes. It is worth mentioning that the (001) reflection at 6.9 Å has been related to the formation of a superstructure due to re-arrengement of the surface, as this reflection should not appear in either the hexagonal or the monoclinic HAp because of extinction conditions.[S6]

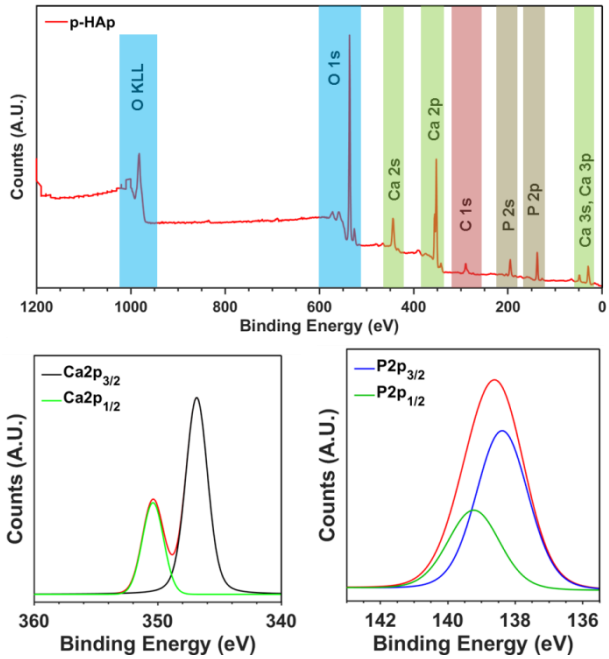

Figure S4. Stability study of the p-HAp catalyst before and after the reaction. The Raman spectra of the ν_1 peak in the region of 920 – 1000 cm^{-1} has been performed to confirm that the structural stability of the catalyst is not altered during the reaction. Little variations of the crystal phase distributions are expected, because of the fact that (and confirmed by HRTEM images) these distortions occur at the surface of the HAp catalysts instead of being a global bulk phenomena.

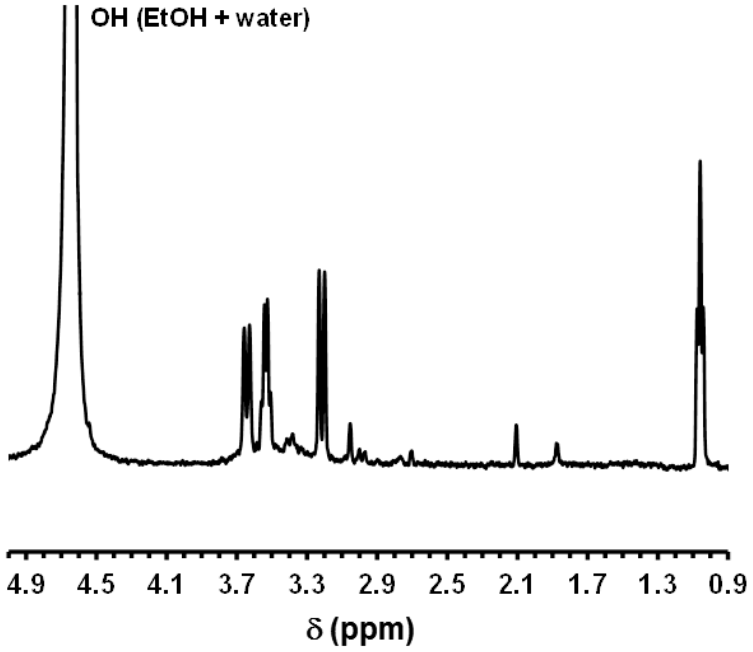

Figure S5. ^{1}H NMR spectra of the solution obtained from the dissolved catalyst. The reaction was conducted for 72 h using CO_2 (3 bar), CH_4 (3 bar) and H_2O (1 mL) at 95 ºC under UV radiation and p-HAp/coat as catalyst. The reacted catalysts were dissolved in an aqueous solution with 100 mM HCl and 50 mM NaCl.

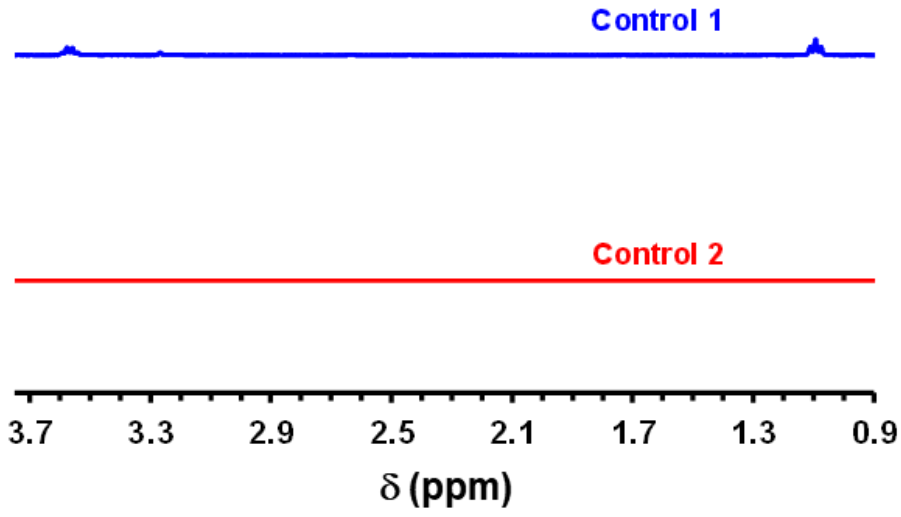

Figure S6. ^{1}H NMR spectra of the liquid water after 72 h using CO_2 (3 bar), CH_4 (3 bar) and H_2O (1 mL) at 95 ºC under UV radiation (control 1) and without using UV radiation (control 2). No catalyst was used for these reactions.

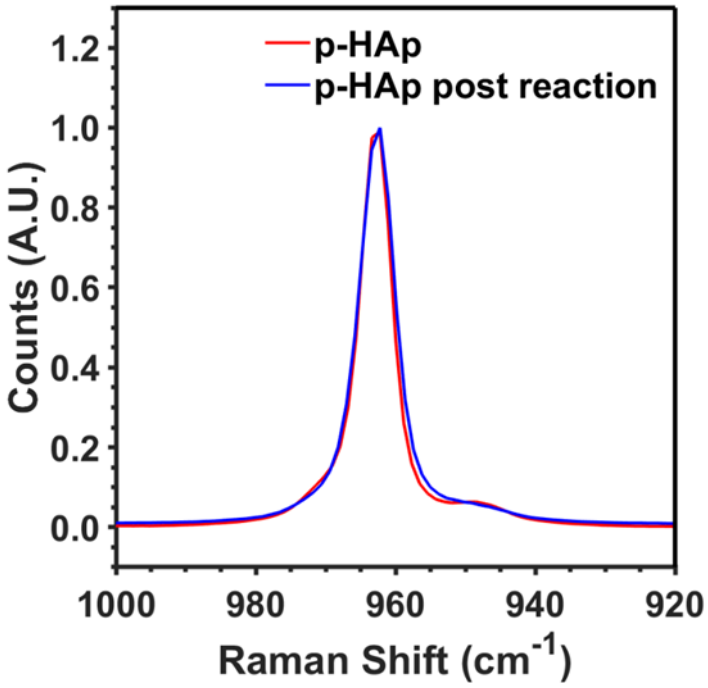

Figure S7. Stability study of the p-HAp catalyst before and after the reaction. The Raman spectra of the ν_1 peak in the region of 920 – 1000 cm^{-1} has been performed to confirm that the structural stability of the catalyst is not altered during the reaction. Little variations of the crystal phase distributions are expected, because of the fact that (and confirmed by HRTEM images) these distortions occur at the surface of the HAp catalysts instead of being a global bulk phenomena.

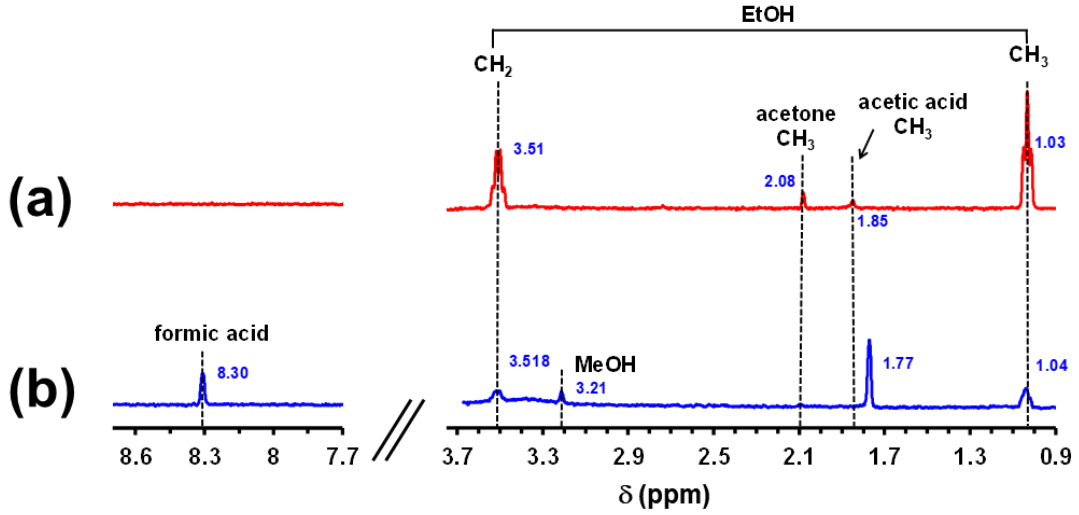

Figure S8. ^1H NMR spectra of the reaction products achieved after 72 h using CO_2 (3 bar), CH_4 (3 bar) and H_2O (1 mL) at 95 ºC under UV radiation and p-HAp as catalyst: (a) Analysis of the solution obtained by dissolving the catalyst with 100 mM HCl and 50 mM NaCl; and (b) analysis of liquid water incorporated to the reaction chamber.

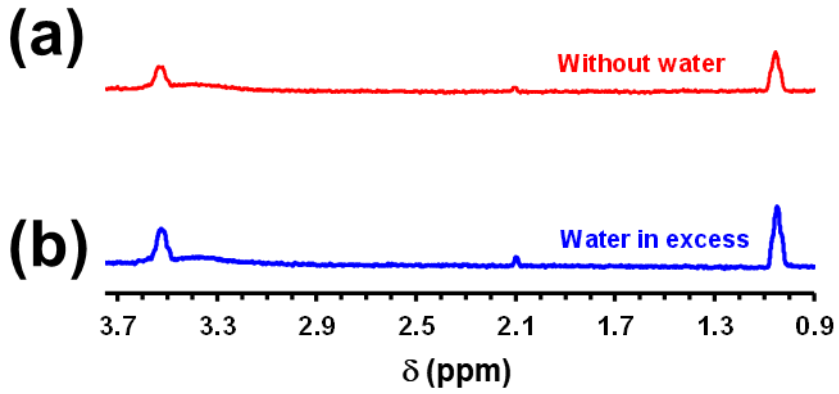

Figure S9. ^{1}H NMR spectra of the solutions obtained from the dissolved catalysts. The reactions were conducted for 72 h using CO_2 (3 bar) and CH_4 (3 bar) at 95 ºC under UV radiation and p-HAp as catalyst (a) in absence of water (b) with an excess of water.